arXiv:1512.05494v1 [cond-mat.mes-hall] 17 Dec 2015

# Quantum Anomalous Hall Effect in a Perovskite and Inverse-Perovskite Sandwich Structure

Long-Hua Wu[1,2*] and Qi-Feng Liang[1,3], and Xiao Hu[1,2†]
[1] *International Center for Materials Nanoarchitectonics (WPI-MANA), National Institute for Materials Science, Tsukuba 305-0044, Japan*
[2] *Graduate School of Pure and Applied Sciences, University of Tsukuba, Tsukuba 305-8571, Japan*
[3] *Department of Physics, Shaoxing University, Shaoxing 312000, China*

Based on first-principles calculations, we propose a sandwich structure composed of a G-type antiferromagnetic (AFM) Mott insulator $LaCrO_3$ grown along the [001] direction with one atomic layer replaced by an inverse-perovskite material $Sr_3PbO$. We show that the system is in a topologically nontrivial phase characterized by simultaneous nonzero charge and spin Chern numbers, which can support a spin-polarized and dissipationless edge current in a finite system. Since these two materials are stable in bulk and match each other with only small lattice distortions, the composite material is expected easy to synthesize.

## I. INTRODUCTION

Discovery of the quantum Hall effect (QHE) by von Klitzing has opened a new era in condensed matter physics[1]. It is revealed that the quantization of Hall conductance is a manifestation of topologically nontrivial Bloch wavefunctions[2]. Topological matters have various promising applications in many fields, such as fault-tolerant topological quantum computations[3–7], spintronics[8,9] and photonics[10–12].

The quantum spin Hall effect (QSHE) was first predicted theoretically in graphene[13–15] and later studied in a two-dimensional (2D) HgTe quantum well both theoretically[16,17] and experimentally[18]. A 3D topological insulator $Bi_{1-x}Sb_x$ and its family members were also reported[19–21]. Breaking time-reversal symmetry can drive a topological insulator into the quantum anomalous Hall effect (QAHE)[22,23]. There are two categories of the QAHE classified by the spin Chern number[24,25]. One subclass of the QAHE is characterized by a vanishing spin Chern number. The Cr-doped $Bi_2Se_3$ thin film[23,26,27] belongs to this class, where the topological band gap is opened by hybridizations between the spin-up and -down channels. The other subclass of the QAHE has a nonzero spin Chern number. One representative material is the Mn-doped HgTe[28], where the $s$-type electrons of Hg and the $p$-type holes of Te experience opposite $g$-factors when they couple with the $d$ electrons of Mn. The opposite exchange fields felt by the $s$ and $p$ orbitals enlarge the energy gap in one spin channel, and close and then reopen the energy gap in the other spin channel, which induces a nontrivial topology in the latter spin channel due to the band inversion mechanism[16,28], for a large enough $g$-factor. However, its experimental realization turns out to be difficult due to the paramagnetic state of Mn spins. Two other materials are proposed to realize the QAHE with nonzero spin Chern numbers in honeycomb lattice, a silicene sheet sandwiched by two ferromagnets with magnetization directions aligned antiparallelly[29], and a perovskite material $LaCrO_3$ grown along the [111] direction with Cr atoms replaced by Ag or Au in one atomic layer[23,30]. In both systems, in addition to the anti-ferromagnetic (AFM) exchange field and spin-orbit coupling (SOC), a strong electric field is required to break the inversion symmetry in order to realize the QAHE. For the former one, the weak SOC of silicene limits the novel QAHE to low temperatures, while for the latter one, growth of the perovskite material along the [111] direction seems to be difficult.

In the present work, we propose a new material to realize the second subclass of the QAHE without any extrinsic operation and easy to synthesize. It is based on $LaCrO_3$ grown along the [001] direction, where we insert one atomic layer of an inverse-perovskite material $Sr_3PbO$[31,32] such that the Pb atom feels the exchange field established by the Cr atoms in the parent material. With first-principles calculations, we reveal that there is a band inversion at the $\Gamma$ point between the $d$ orbital of Cr and the $p$ orbital of Pb in the spin-up channel induced by the SOC, whereas the spin-down bands are pushed far away from the Fermi level by the AFM exchange field. Constructing an effective low-energy Hamiltonian, we explicitly show that the system is characterized by simultaneous nonzero charge and spin Chern numbers. Projecting the bands near the Fermi level onto the subspace composed of the spin-up $d$ and $p$ orbitals by maximally localized Wannier functions[33], we confirm that a spin-polarized and dissipationless current flows along the edge of a finite sample. Since these two materials are stable in bulk and match each other with small lattice distortions, the composite material is expected easy to synthesize.

## II. FIRST-PRINCIPLES CALCULATIONS

The parent material $LaCrO_3$ exhibits the perovskite structure with formula $ABO_3$, where the oxygen atoms form an octahedron surrounding the B atom. It is a well-known Mott insulator with a large energy gap $\sim$3 eV, carrying the G-type AFM order, where the spin moment of any Cr aligns opposite to all its neighbors. On the other hand, the material $Sr_3PbO$ shows the inverse-

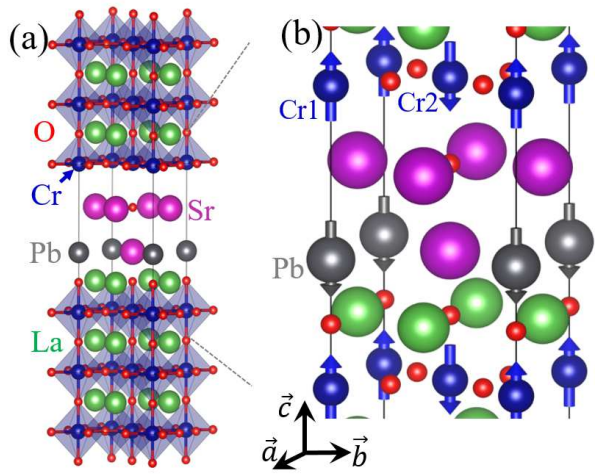


FIG. 1. (Color online) (a) Crystal structure of bulk $LaCrO_3$ grown along the [001] direction with one atomic layer replaced by $Sr_3PbO$. (b) Enlarged interface between $LaCrO_3$ and $Sr_3PbO$ with grey and blue arrows representing spin moments on Pb and Cr sites, respectively. $\vec{a}$, $\vec{b}$ and $\vec{c}$ are lattice vectors.

perovskite structure with formula $A_3BO$, where the A atoms form an octahedron surrounding the oxygen. It was revealed recently that there is a topological band gap in bulk $Sr_3PbO$[34,35]. We notice that the $\vec{a}$-$\vec{b}$ plane lattice constant is 3.88 Å for $LaCrO_3$, and 5.15 Å for $Sr_3PbO$, different from each other by a factor close to $\sqrt{2}$. Therefore, with a $\pi/4$ rotation around the common $\vec{c}$ axis, these two materials match each other quite well [see Figs. 1(a) and (b)]. At the interface the oxygen of $Sr_3PbO$ completes the $CrO_6$ octahedron of the perovskite structure [see Fig. 1(b)], which minimizes the distortion to the two materials when grown together. As shown in Fig. 1(b) zoom-in at the interface, there are two types of Cr atoms in each $CrO_2$ unit cell, where Cr1 sits at the corners of the square and above the Pb atom in the $\vec{c}$ axis, whereas Cr2 sits at the center of square and above the oxygen.

We have performed first-principles calculations by using density functional theory (DFT) implemented in the Vienna *Ab-initio* Simulation Package (VASP)[36], which uses the projected augmented wave (PAW) method[37,38]. The exchange correlation potential is described by the generalized gradient approximation (GGA) of Perdew-Burke-Ernzerhof (PBE) type[39]. The cut-off energy of the plane waves is chosen to be 500 eV. The Brillouin zone is meshed into a $10 \times 10 \times 1$ grid using the Monkhorst-Pack method. The Hubbard-U term is included for the Cr-3$d$ electrons with $U = 5.0$ eV and $J = 0.5$ eV[40] by using the Dudarev method. For the lattice structure, we take $a = b = 5.48$ Å ($= \sqrt{2} \times 3.88$ Å) and $c_{\mathrm{LaCrO}} = 3.88$ Å. The height of the inserted $Sr_3PbO$ layer is determined by a relaxation process to achieve the minimal energy: $c_{\mathrm{SrPbO}} = 5.46$ Å, the distance from the Pb atom to the Cr just above it (that to the Cr below it is $c_{\mathrm{LaCrO}}$). Afterwards, the positions of atoms are determined by a second relaxation process with all lattice constants fixed. In both processes, the criterion on forces between atoms is set to below 0.01 eV/Å. The results shown below are for a superlattice structure with five layers of $LaCrO_3$ and one atomic layer of $Sr_3PbO$. We confirm that the results remain unchanged as far as the number of $LaCrO_3$ layers is above five and for $U_{\mathrm{eff}} = U - J > 3.5$ eV.

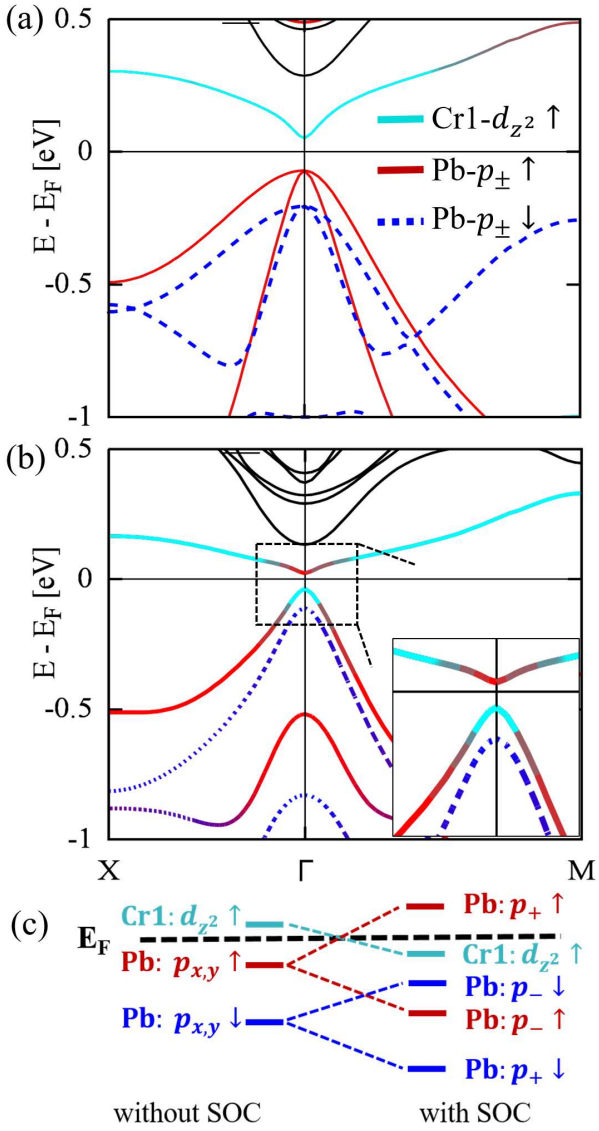


FIG. 2. (Color online) Band structure of the supercell shown in Fig. 1 without (a) and with (b) SOC. Solid cyan, solid red and dashed blue curves are for Cr1-$d^{\uparrow}_{z^2}$, Pb-$p^{\uparrow}_{\pm}$ and Pb-$p^{\downarrow}_{\pm}$ orbitals, respectively. Other colors indicate their hybridizations. (c) Schematic band evolution of Pb-$p_{x,y}$ and Cr-$d_{z^2}$ at the Γ point caused by SOC.

Without SOC, we find a band gap 0.18 eV at the Γ point. As shown in Fig. 2(a), the topmost valence band is occupied by the spin-up $p_{\pm}(= p_x \pm ip_y)$ orbitals of Pb, and the lowest conduction band is contributed by the spin-up $d_{z^2}$ of Cr1. The reason for this band ar-

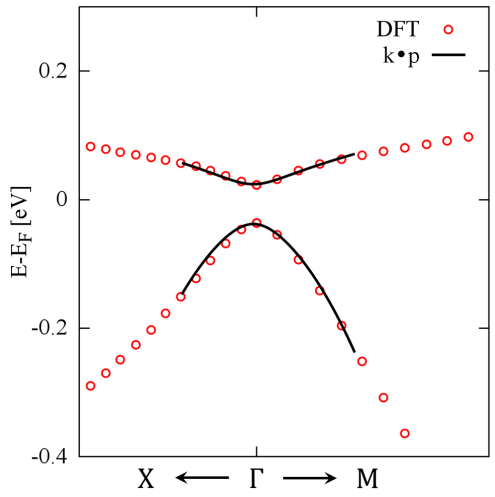


FIG. 3. (Color online) Energy dispersion around the Γ point fitted by the 2×2 $\mathbf{k}\cdot\mathbf{P}$ Hamiltonian (4) on the basis $[d^{\uparrow}_{z^2}, p^{\uparrow}_{+}]$. The fitted curves collapse with the DFT results within the region $|k_x| \leq 0.08\frac{2\pi}{a}$ and $|k_y| \leq 0.08\frac{2\pi}{b}$, where $a$ and $b$ are lattice constants given in text.

rangement is that the Cr1 atom does not live in a closed octahedron due to the absence of an oxygen in the corner of $Sr_2O$ layer as shown in Fig. 1(b), which weakens the crystal field splitting and lowers the energy of the unoccupied Cr1-$d_{z^2}$ band, whereas the Cr2 shares one oxygen with $Sr_3PbO$, thus is closed by a complete oxygen octahedron, which keeps its $d_{z^2}$ far away from the Fermi level. Therefore, only the spin-up Cr1-$d_{z^2}$ band appears just above the Fermi level, in contrast to the original Mott insulator. Meanwhile, the Pb acquires a magnetic moment $0.19\mu_B$ polarized downwards [see Fig. 1(b)], which matches the overall AFM order of $LaCrO_3$ and splits the spin-up and spin-down $p$ orbitals of Pb [see Fig. 2(a)]. In this way, both the topmost valence band and the bottommost conduction band are occupied by the spin-up channel. We notice that the total magnetic moment in the present system is compensated to zero, distinct from the Cr-doped $Bi_2Se_3$[23,26].

The band structure of the material is then calculated with SOC turned on, which lifts the degeneracy of the $p_+$ and $p_-$ bands in both spin channels. Remarkably, the strong SOC of the heavy element Pb pushes the $p_+$ orbital with up spin even above the Fermi energy $E_F$ around the Γ point as displayed in Figs. 2(b) and (c). The Cr1-$d_{z^2}$ orbital with up spin then has to sink across the Fermi level partially in order to maintain the charge neutrality of the system, which causes a band inversion between the $p$ and $d$ orbitals around the Γ point, as shown in Fig. 2(b). An energy gap of 59 meV is observed according to the first-principles calculations.

## III. EFFECTIVE LOW-ENERGY MODEL

We now derive an effective low-energy $\mathbf{k}\cdot\mathbf{P}$ Hamiltonian to describe topological properties of the system. Noticing that the topological band gap is opened by hybridizations between the spin-up $p_+$ orbital of Pb and the spin-up $d_{z^2}$ orbital of Cr1, it is then reasonable to take these two orbitals as a basis to construct a 2×2 Hamiltonian. For simplicity, we denote the two orbitals as $\Gamma_1 = d^{\uparrow}_{z^2}$ and $\Gamma_2 = p^{\uparrow}_{+}$. The effective $\mathbf{k}\cdot\mathbf{P}$ Hamiltonian around the Γ point is

$$H(\mathbf{k}) = H_0 + H' \tag{1}$$

on the basis $[\Gamma_1, \Gamma_2]$, where

$$H_0 = \begin{pmatrix} \epsilon_1 + \gamma_1\mathbf{k}^2 & 0 \\ 0 & \epsilon_2 + \gamma_2\mathbf{k}^2 \end{pmatrix} \tag{2}$$

and $H' = \mathbf{k}\cdot\mathbf{P} = (k_-P_+ + k_+P_-)/2$ is the perturbation term with $k_\pm = k_x \pm ik_y$ and $P_\pm = P_x \pm iP_y$ ($P_{x/y}$ is the momentum operator in the $x/y$ direction). Since the crystal is symmetric with respect to the $C_4$ rotation around the $\vec{c}$ axis, $H'$ must be invariant under the $C_4 = e^{-i\frac{2\pi}{4}J_z}$ transformation, where $J_z$ the is the $z$-component of the total angular momentum. The symmetry constraint allows us to determine nonzero entries of $H'$[41]. It is easy to check that $C_4\Gamma_1 = e^{-i\frac{\pi}{4}}\Gamma_1$ and $C_4\Gamma_2 = e^{-i\frac{3\pi}{4}}\Gamma_2$ because $J_z = 1/2$ and $3/2$ for $\Gamma_1$ and $\Gamma_2$ respectively. Since

$$\begin{aligned} \langle\Gamma_1|P_+|\Gamma_2\rangle &= \langle\Gamma_1|C_4^\dagger C_4 P_+ C_4^\dagger C_4|\Gamma_2\rangle \\ &= \langle\Gamma_1|e^{i\frac{\pi}{4}}e^{-i\frac{\pi}{2}}P_+e^{-i\frac{3\pi}{4}}|\Gamma_2\rangle \\ &= -\langle\Gamma_1|P_+|\Gamma_2\rangle, \end{aligned} \tag{3}$$

$\langle\Gamma_1|k_-P_+|\Gamma_2\rangle$ must vanish. Performing similar calculations for all other terms, we arrive at the Hamiltonian respecting the crystal symmetry

$$H(\mathbf{k}) = \left(\epsilon_0 + \gamma_0 k^2\right) I_{2\times2} + \begin{pmatrix} \epsilon + \gamma\mathbf{k}^2 & \alpha k_+ \\ \alpha^* k_- & -\epsilon - \gamma\mathbf{k}^2 \end{pmatrix} \tag{4}$$

up to the lowest orders of $\mathbf{k}$, with $\epsilon_0 = (\epsilon_1 + \epsilon_2)/2$, $\epsilon = (\epsilon_1 - \epsilon_2)/2$, $\gamma_0 = (\gamma_1 + \gamma_2)/2$ and $\gamma = (\gamma_1 - \gamma_2)/2$. By fitting the energy dispersion of $H(\mathbf{k})$ in Eq. (4) against the first-principles results given in Fig. 2(b), we obtain the parameters as follows: $\epsilon_0 = -0.007$ eV, $\gamma_0 = -7.8$ eV·Å$^2$, $\epsilon = -0.031$ eV, $\gamma = 9.0$ eV·Å$^2$ and $\alpha = 1.45$ eV·Å (see Fig. 3). Since $\epsilon$ and $\gamma$ take opposite signs, the electronic wavefunction of the spin-up channel becomes topologically nontrivial due to the band inversion mechanism with Chern number $C_\uparrow = 1$. Since the spin-down electronic bands are kept far away from the Fermi level [see Figs. 2(b) and (c)], one clearly has $C_\downarrow = 0$. It is therefore confirmed that the system is characterized by simultaneous charge and spin Chern numbers: $C_c = C_\uparrow + C_\downarrow = 1$ and $C_s = C_\uparrow - C_\downarrow = 1$.

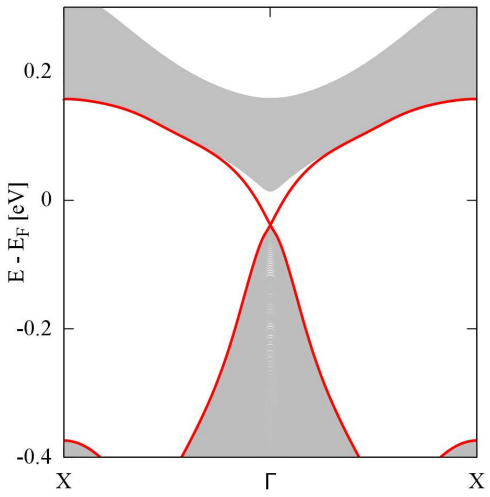


FIG. 4. (Color online) Band structure for a slab of the system shown in Fig. 1 based on Wannierized wavefunctions downfolded from the results of the first-principles calculations in Fig. 2(b). Red curves are for topological edge states in the spin-up channel, and grey ones are for bulk states.

## IV. TOPOLOGICAL EDGE STATES

The nontrivial topology gives rise to gapless edge states in a finite sample. To illustrate this feature, we calculate the dispersion relation for a slab of the topological material with $100a$ along the $\vec{a}$ axis and infinite along the $\vec{b}$ axis (see Fig. 1). Since the bulk bands close to the Fermi level are mainly contributed by the Pb-$p_x$, Pb-$p_y$ and Cr1-$d_{z^2}$ orbitals, it is reasonable to downfold the wavefunctions obtained by the first-principles calculations in Fig. 2(b) onto these three orbitals. Employing the maximally-localized Wannier functions[33], we obtain the hopping integrals within the six-dimensional subspace including the spin degree of freedom. It is then straightforward to calculate the band structure of the slab system. As shown in Fig. 4, a gapless edge state with up spin appears inside the bulk gap, manifesting the nontrivial topology of the present system.

## V. DISCUSSION

Liu[42] proposed a 3D spinless model for a layered square lattice with A-type AFM (intra-plane ferromagnetic and inter-plane AFM orderings). At each lattice site, there are three orbitals: $s$, $p_x$ and $p_y$. Each layer can be driven into a QAHE in a same way as that for the Mn-doped HgTe[28]. Since every two adjacent layers have opposite magnetic moments, their chiral edge states propagate counter to each other. Therefore, the system can be viewed as a stack of quantum spin Hall insulators [see also[43]], where the combination of the time-reversal and the primitive-lattice translational symmetries is preserved. In contrast, all symmetries are broken in our system, giving rise to a Chern insulator.

## VI. CONCLUSION

We propose a novel topological material composed of the $LaCrO_3$ of perovskite structure grown along the [001] direction with one atomic layer replaced by an inverse-perovskite material $Sr_3PbO$. Based on first-principles calculations and an effective low-energy Hamiltonian, we demonstrate that the topological state is characterized by simultaneous nonzero charge and spin Chern numbers, which can support a spin-polarized and dissipationless edge current in a finite sample. Supported by the anti-ferromagnetic exchange field and spin-orbit coupling inherent in the compounds, no extrinsic operation is required for achieving the novel topological state. Importantly, these two materials are stable in bulk and match each other with only small lattice distortions, which makes the composite material easy to synthesize.

## ACKNOWLEDGMENTS

This work was supported by the WPI Initiative on Materials Nanoarchitectonics, Ministry of Education, Culture, Sports, Science and Technology of Japan. QFL acknowledges support from the National Natural Science Foundation of China (No.11574215) and the Scientific Research Foundation for the Returned Overseas Chinese Scholars, State Education Ministry.

* Wu.Longhua@nims.go.jp
† Hu.Xiao@nims.go.jp

[1] K. v. Klitzing, G. Dorda, and M. Pepper, Phys. Rev. Lett. **45**, 494 (1980).
[2] D. J. Thouless, M. Kohmoto, M. P. Nightingale, and M. den Nijs, Phys. Rev. Lett. **49**, 405 (1982).
[3] C. Nayak, S. H. Simon, A. Stern, M. Freedman, and S. Das Sarma, Rev. Mod. Phys. **80**, 1083 (2008).
[4] T. D. Stanescu and S. Tewari, J. Phys.: Condens. Matter **25**, 233201 (2013).
[5] C. W. J. Beenakker, Annu. Rev. Condens. Matter Phys. **4**, 113 (2013).
[6] L.-H. Wu, Q.-F. Liang, and X. Hu, Sci. Technol. Adv. Mater. **15**, 064402 (2014).
[7] T. Kawakami and X. Hu, Phys. Rev. Lett. **115**, 177001 (2015).
[8] O. V. Yazyev, J. E. Moore, and S. G. Louie, Phys. Rev. Lett. **105**, 266806 (2010).
[9] D. Pesin and A. H. MacDonald, Nat. Mater. **11**, 409 (2012).

[10] F. D. M. Haldane and S. Raghu, Phys. Rev. Lett. **100**, 013904 (2008).
[11] A. B. Khanikaev, S. H. Mousavi, W.-K. Tse, M. Kargarian, A. H. MacDonald, and G. Shvets, Nat. Mater. **12**, 233 (2013).
[12] L.-H. Wu and X. Hu, Phys. Rev. Lett. **114**, 223901 (2015).
[13] C. L. Kane and E. J. Mele, Phys. Rev. Lett. **95**, 226801 (2005).
[14] C. L. Kane and E. J. Mele, Phys. Rev. Lett. **95**, 146802 (2005).
[15] M. Z. Hasan and C. L. Kane, Rev. Mod. Phys. **82**, 3045 (2010).
[16] B. A. Bernevig, T. L. Hughes, and S.-C. Zhang, Science **314**, 1757 (2006).
[17] X.-L. Qi and S.-C. Zhang, Rev. Mod. Phys. **83**, 1057 (2011).
[18] M. König, S. Wiedmann, C. Brüne, A. Roth, H. Buhmann, L. W. Molenkamp, X.-L. Qi, and S.-C. Zhang, Science **318**, 766 (2007).
[19] D. Hsieh, D. Qian, L. Wray, Y. Xia, Y. S. Hor, R. J. Cava, and M. Z. Hasan, Nature **452**, 970 (2008).
[20] H. Zhang, C.-X. Liu, X.-L. Qi, X. Dai, Z. Fang, and S.-C. Zhang, Nat. Phys. **5**, 438 (2009).
[21] Y. Ando, J. Phys. Soc. Jpn. **82**, 102001 (2013).
[22] F. D. M. Haldane, Phys. Rev. Lett. **61**, 2015 (1988).
[23] H.-M. Weng, R. Yu, X. Hu, X. Dai, and Z. Fang, Adv. Phys. **64**, 227 (2015).
[24] E. Prodan, Phys. Rev. B **80**, 125327 (2009).
[25] Y. Yang, Z. Xu, L. Sheng, B. Wang, D. Y. Xing, and D. N. Sheng, Phys. Rev. Lett. **107**, 066602 (2011).
[26] R. Yu, W. Zhang, H.-J. Zhang, S.-C. Zhang, X. Dai, and Z. Fang, Science **329**, 61 (2010).
[27] C.-Z. Chang, J. Zhang, X. Feng, J. Shen, Z. Zhang, M. Guo, K. Li, Y. Ou, P. Wei, L.-L. Wang, Z.-Q. Ji, Y. Feng, S. Ji, X. Chen, J. Jia, X. Dai, Z. Fang, S.-C. Zhang, K. He, Y. Wang, L. Lu, X.-C. Ma, and Q.-K. Xue, Science **340**, 167 (2013).
[28] C.-X. Liu, X.-L. Qi, X. Dai, Z. Fang, and S.-C. Zhang, Phys. Rev. Lett. **101**, 146802 (2008).
[29] M. Ezawa, Phys. Rev. B **87**, 155415 (2013).
[30] Q.-F. Liang, L.-H. Wu, and X. Hu, New J. Phys. **15**, 063031 (2013)
[31] A. Widera and H. Schäfer, Mater. Res. Bull. **15**, 1805 (1980).
[32] T. Kariyado and M. Ogata, J. Phys. Soc. Jpn. **81**, 064701 (2012).
[33] A. A. Mostofi, J. R. Yates, Y.-S. Lee, I. Souza, D. Vanderbilt, and N. Marzari, Comput. Phys. Commun. **178**, 685 (2008).
[34] M. Klintenberg, arXiv:1007.4838.
[35] T. H. Hsieh, J. Liu, and L. Fu, Phys. Rev. B **90**, 081112(R) (2014).
[36] G. Kresse and J. Furthmüller, Phys. Rev. B **54**, 11169 (1996).
[37] P. E. Blöchl, Phys. Rev. B **50**, 17953 (1994).
[38] G. Kresse and D. Joubert, Phys. Rev. B **59**, 1758 (1999).
[39] J. P. Perdew, K. Burke, and M. Ernzerhof, Phys. Rev. Lett. **77**, 3865 (1996).
[40] Z. Yang, Z. Huang, L. Ye, and X. Xie, Phys. Rev. B **60**, 15674 (1999).
[41] R. Yu, H.-M. Weng, X. Hu, Z. Fang, and X. Dai, New J. Phys. **17**, 023012 (2015).
[42] C.-X. Liu, arXiv:1304.6455.
[43] R. S. K. Mong, A. M. Essin, and J. E. Moore, Phys. Rev. B **81**, 245209 (2010).